



HAL
open science

Solar type IV burst spectral fine structures . I. Observations

Henry Aurass, Karl-Ludwig Klein, E. Ya. Zlotnik, V. V. Zaitsev

► **To cite this version:**

Henry Aurass, Karl-Ludwig Klein, E. Ya. Zlotnik, V. V. Zaitsev. Solar type IV burst spectral fine structures . I. Observations. *Astronomy and Astrophysics - A&A*, 2003, 410, pp.1001-1010. 10.1051/0004-6361:20031249 . hal-03801300

HAL Id: hal-03801300

<https://hal.science/hal-03801300>

Submitted on 13 Oct 2022

HAL is a multi-disciplinary open access archive for the deposit and dissemination of scientific research documents, whether they are published or not. The documents may come from teaching and research institutions in France or abroad, or from public or private research centers.

L'archive ouverte pluridisciplinaire **HAL**, est destinée au dépôt et à la diffusion de documents scientifiques de niveau recherche, publiés ou non, émanant des établissements d'enseignement et de recherche français ou étrangers, des laboratoires publics ou privés.

Solar type IV burst spectral fine structures

I. Observations

H. Aurass¹, K.-L. Klein², E. Ya. Zlotnik³, and V. V. Zaitsev³

¹ Astrophysical Institute Potsdam, 14482 Potsdam, Germany

² Paris-Meudon Observatory, LESIA, CNRS-UMR 8109, 92195 Meudon, France

³ Institute of Applied Physics RAS, 603600 Nizhny Novgorod, Russia

Received 2 June 2003 / Accepted 28 July 2003

Abstract. The fine structures (FS) of solar type IV radio bursts are of principal interest for flare plasma diagnostics in the low corona. In this paper we give an observational (Part I) and theoretical (Paper II) treatment of broad band radio pulsations (BBP) and zebra patterns (ZP) in a well observed flaring sigmoidal loop system of AR 7792 on 25 October 1994. We present comprehensive meter-decimeter radio spectral (Astrophysical Institute Potsdam, AIP) and meter wave heliographic (Nançay Radio Heliograph of Paris-Meudon Observatory, NRH) observations. Spectral and spatial properties of FS elements (one pulsation pulse, one single zebra stripe) as well as a statistical analysis for the whole fine structure event are presented. The source sites are compared with soft X-ray images of the flare, and with force-free extrapolated coronal magnetic fields. Both FS sources occur in a common diverging loop structure with a turning height of about 70 Mm. The BBP source is shown to appear (if seen along the loop axis) nearer to the injection site of the electrons than the ZP source. BBP do show high frequency drift ($\approx -250 \text{ MHz s}^{-1}$). At a given frequency, the projected source speed is $1.1 \times 10^5 \text{ km s}^{-1}$. For ZP, we find a good correlation between the inclination of a single zebra stripe to the heliographic observing frequency level in the dynamic spectrogram, and the speed of the simultaneously observed projected source motion at this frequency. The direction of the source motion at a given frequency is on average found to be perpendicular between BBP and ZP sources. During a time interval of 90 s the BBP source consists in its lower part (higher observing frequencies) of a widely spaced double source. Despite a source distance of 360 Mm both subsources are highly correlated and thus probably simultaneously driven. We come to the conclusion that both fine structures are emitted during repeated electron beam injection into an asymmetric magnetic trap configuration between a footpoint in the leading spot of AR 7792 and a trailing more dispersed footpoint. In Paper II we will show that the specifications derived from the data allow for selecting one out of several competing fine structure models which explains the simultaneous formation of BBP and ZP in the same loop structure.

Key words. Sun: flares – Sun: corona – Sun: radio radiation – Sun: magnetic fields

1. Introduction

The radio burst emission of the Sun in the meter-decimeter waveband is known to be rather varied (McLean & Labrum 1985 for general reference). It often reveals spectral fine structures (FS) on dynamic spectra, that is narrowband features and fast temporal changes¹. To some extent, studying such very specific signatures can give precise information about physical processes responsible for the observed radio emission, as well as about the necessary conditions in the coronal sources. An instructive example is the type IV burst radio emission: a broad band smooth type IV continuum can well be understood as synchrotron radiation of accelerated electrons. However, this

changed because of the discovery of FS frequently superposed on the source of the continuum background. There were parallel drifting narrowband stripes (zebra pattern, ZP), broad band quasi-periodic modulations of radio brightness (BBP, pulsations with periods from 0.1...10 s), fiber or intermediate drift bursts, tadpoles, and others (see Slottje 1981). Those continua which are partly structured in frequency and time have probably to be explained by plasma wave mechanisms. Today we know, on the other hand, that e.g. the faint and smooth continua associated frequently with the release of coronal mass ejections (Aurass et al. 1999) are due to synchrotron radiation (Bastian et al. 2001).

In this paper we discuss the origin of ZP and BBP in the October 25, 1994 event. The dynamic spectrum of this event was rich in various kinds of well expressed FS. Our goal is to compare the FS observations with theoretical predictions of

Send offprint requests to: H. Aurass, e-mail: haurass@aip.de

¹ We mean a bandwidth of some percent of the observing frequency, and seconds to subsecond time scale.

possible mechanisms to decide between different explanations. We give to some extent a comprehensive spectral and radio imaging analysis of the elements of the FS (a single pulsation pulse, a single zebra stripe), and thereafter, a statistical evaluation of the FS in the event of interest.

BBPs and ZPs in solar type IV radio emission are rather frequently observed. Early work comes from Elgaroy (1959), Young et al. (1961), Ellis (1969), Rosenberg (1970), McLean & Sheridan (1973), Gotwols (1973). Numerous examples are given in Slottje (1972, 1981), Chernov et al. (1975), Kuijpers (1975a,b), Abrami & Koren (1978), Aurass & Chernov (1983), Aschwanden & Benz (1986), Aurass (1999), and others. As a rule, and at first glance, in the beginning of the event BBPs arise, and after some time delay they are superposed by ZP starting from the low frequency edge of the continuum. The time delay ranges from some ten seconds to a few minutes. This means the FS can occur not only in the first minutes of the impulsive flare phase, but also well within the gradual phase. Sometimes they appear in the gradual decay of long duration events hours after the impulsive flare phase (Aurass et al. 1987; Chernov et al. 1998).

We limit ourselves to the consideration of BBPs with non-drifting spectral envelopes. This means we are going to discuss those BBP without systematically drifting high- and low-frequency boundaries. We know from other recent work (e.g. Karlicky et al. 2002; Khan et al. 2002) that the pulsations with a drifting envelope are associated with soft X-ray blob ejections, and can well be understood by repeated electron beam injection or by magnetoplasma blob oscillations.

Decimetric and metric BBP are believed to be associated with either magnetohydrodynamic (MHD) oscillations of the source of radio emission, or with periodic regimes of particle acceleration (Kuijpers 1980; Aschwanden 1987). For the ZP, two approaches are mainly discussed in the literature: the enhanced excitation of plasma waves in double plasma resonance regions of a nonuniform source, and their consequent transformation into electromagnetic radiation (Kuijpers 1975a,b; Zheleznyakov & Zlotnik 1975a,b; Winglee & Dulk 1986); or the scattering of a uniform plasma wave continuum on a structured field of whistler waves (Chernov 1976; Chernov et al. 1998).

From the theoretical point of view, BBP and ZP are considered as independent phenomena in type IV radio emission. This disagrees with the experience that frequently both phenomena occur in the same event and seemingly in some typical sequence.

In this paper (Paper I) we present the observations and summarize essential facts about BBPs and ZPs. We give detailed spectral and imaging information about a single pulsation pulse, a single zebra stripe, and also statistical information about both phenomena. So we proceed further than it was possible in early work about imaging radio pulsations (Kai & Takayanaki 1973; Trotter et al. 1981²). In a second part (Paper II) the different mechanisms of pulsations are reconsidered and compared with a source model fitted to the observational facts. Further, the mechanisms of ZP formation are

critically revisited. At the end of Paper II we summarize our results about a common source of BBP and ZP in solar radio bursts.

2. Observations

In this paper we discuss radio observations of the Astrophysical Institute Potsdam (AIP) – spectral data between 40 and 800 MHz (Mann et al. 1992) – and the Paris-Meudon Observatory, Nançay Multifrequency Radio Heliograph (NRH, The Radioheliograph Group 1993). Both data sets complement each other and yield in the time window 9–15 UT the best available coverage of the meter wave radio sun, as already demonstrated in a series of previous papers (e.g. Aurass & Klein 1997; Klein et al. 1997). Other relevant data sources (*Yohkoh* soft X-ray telescope images, Kitt Peak magnetogram data) have already been introduced in previous work about the event of interest (e.g. Aurass et al. 1999).

The Potsdam spectrometer observes the sun using four swept receivers and four independent aerials to obtain a spectral resolution of 0.1..0.8 MHz with a sweep rate of ≈ 0.1 s and a sensitivity comparable to the French radio heliograph. To enhance the resolution of the instrument it is combined with two multichannel receivers (Aurass et al. 2000). One is a 180 channel polarimeter covering 22 MHz centered around 236 or 327 MHz (not available for the event of interest), the other a 48 channel radiometer, 1 MHz channel bandwidth, working between 693 and 740 MHz with one order of magnitude higher time resolution (0.01 s).

The Nançay Multifrequency Radio Heliograph images the sun at five frequencies (164, 236.6, 327, 410, 435 MHz) and a time resolution of up to 0.01 s. At the lowest frequency a spatial resolution (half power beam width) of ≥ 1 arcmin is achieved. The instrument resolves all sources of interest in the given event. In 1994, the NRH still recorded two independent scans of the disc, one projected to the terrestrial NS-, the other to the terrestrial EW direction (NS and EW scan). Due to the aerial system the EW scan is more sensitive than the NS scan. In this paper we draw radio source images by crosses. These give the main axis of a Gaussian source model fit to the independent one-dimensional scan data. The cross represents the fitted model source half power width. If there is no cross given, we mark the source centroid position by a dot to simplify the figures.

2.1. 25 October 1994 – Flare in sigmoid loop structures of AR 7792

The event of interest is a two ribbon flare of importances 1N/C4.7 with remote brightenings in H α . It takes place in a sheared quadrupolar magnetic configuration of NOAA 7792 located S09W12 on 25 October 1994. Soft X-ray images of the flare reveal a sigmoidal pattern of hot and dense loops connecting the flare site with the remote brightening areas. The sigmoidal loop pattern starts to expand and reform in the impulsive flare phase (09:54 UT) and eventually appears as a relaxed combination of three post flare loop systems reaching only lower coronal heights than the preflare loop configuration (10:22 UT).

² During a moving type IV burst.

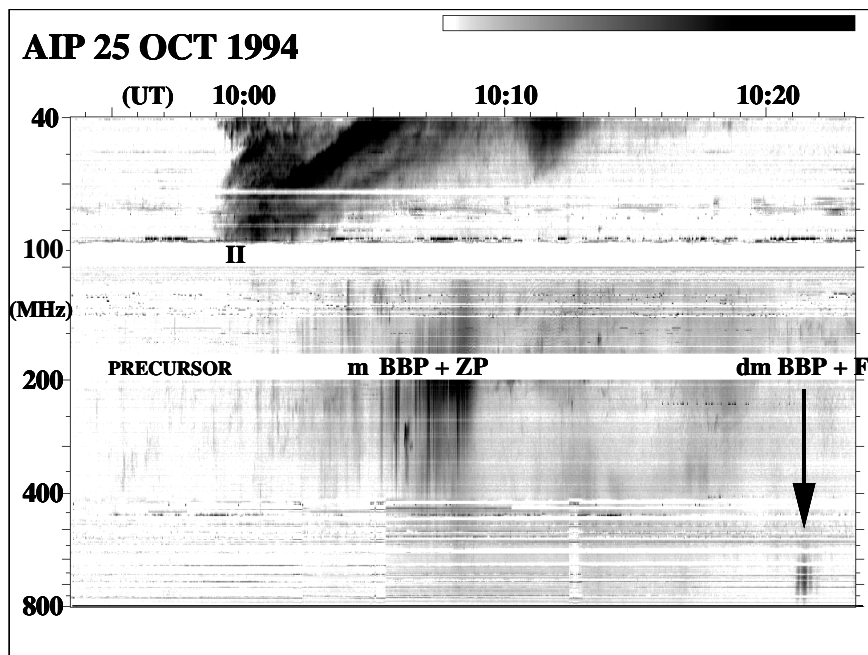


Fig. 1. The 40–800 MHz spectrum of the 25 October 1994 event (AIP). A quiet spectrum is subtracted. Gaps are at 88–108, and 170–200 MHz. Note the type II precursor, the type II burst, and the interval with BBP and ZP. The late dm effect (arrow) contains fast BBP and fiber bursts (F).

AR 7792 is the only active region on the visible disc during the 25 October 1994 flare. Spatially widespread flare-related effects are noticed during and hours after the flare. The flare-related type II/IV radio burst is well resolved into several sub-sources which can nicely be associated with patterns identified in the X-ray images and the magnetic field data. Thus, there is the rare situation that by combining the many different data sets, from a comparison of radio source sites and source timing with the static image of the magnetic field structure in the pre- and postflare active region, the paths of nonthermal electrons during the flare can be reconstructed. This leads to conclusions about the coronal reconfiguration during and after the flare (Aurass et al. 1999).

Figure 1 gives the 40–800 MHz gross radio spectrum of the event. There is a sequence of faint type II burst precursor bursts, followed by a type II burst below 100 MHz. The precursor is accompanied by impulsive phase hard X-ray emission. Manoharan et al. (1996) describe a simultaneous south-westward expansion of the southern semi-sigmoid. In the same time, continuum emission occurs between 100 and 400–600 MHz. Three about 4 min duration continuum enhancements with falling radio intensity occur together with three postflare loop brightenings (Aurass 1999). During the first and strongest enhancement, associated with the middle of three postflare loop systems, the most prominent radio fine structures (BBP and ZP) were observed. Those are our matter of main interest, here. As shown in Fig. 1, the last strong radio feature of the event is a short sequence of decimeter pulses which also contains BBP structures and fiber (intermediate drift) bursts. This late FS patch is out of the frequency range of the NRH. Therefore we do not further consider the fiber bursts in the present paper.

Figure 2 depicts the dominant magnetic structure elements of AR 7792 based on a force-free extrapolation of post-flare

Kitt Peak magnetogram data (redrawn from Aurass et al. 1999). We have plotted a perspective view of field lines with turning heights ≤ 87 Mm. Four groups of field lines were found to be essential. The loop systems LS1 and LS2 form in the top view the soft X-ray sigmoid. In the foreground, there is a number of very low lying connections between a leading parasitic polarity region in the photosphere and the leading main north polarity spot which is also the strong-field end of LS1. The small loop system is denoted by an arrow. We have shown in Aurass et al. (1999) that during the flare there is a strong interaction between the small system and LS1, sometimes also including LS2. All radio FS sources are situated in LS1, partly also in LS2, as we will show in detail later on. In the background of Fig. 2 there is situated the sheared loop arcade. This arcade's eruption causes the type II burst excitation and leads to a distortion of the other three loop systems.

2.2. Radio fine structures

Figure 3 gives an enlargement of the main type IV burst FS pattern – a sweep spectrogram from 10:05–10:09 UT in the frequency range 110–600 MHz. The dominant feature is a continuum patch with a low frequency envelope decaying during the interval from ≥ 170 MHz to ≤ 110 MHz. The pattern can roughly be divided into three time intervals denoted in the spectral gap between 170 and 200 MHz and divided by the stippled vertical lines. At first glance (we will later on specify this) the FS emission starts with two trains of BBP called simple because of its simple radio source structure situated in LS1 (Fig. 2). Each pulse train has a duration of about 35 s. Then there is a gap in the BBP of about 40 s during which some decimetric drift bursts appear dominated by a reverse drift (RS) burst. Its source site is situated in LS2 (Fig. 2). Thereafter the BBP continue stronger than before, having the

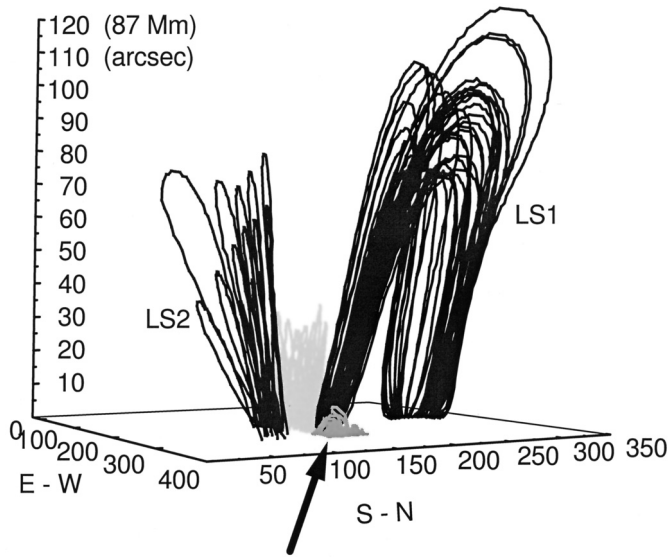


Fig. 2. Perspective view from SW of the force-free extrapolated magnetic field of AR 7792. Field lines are plotted according to the extrapolation data of Aurass et al. (1999). We used Cartesian coordinates, the orientation is given at the axes. Four magnetic systems coexist. The BBP and ZP sources are in and near LS1. LS1 interacts with the smallest system in the foreground (shaded dark grey, marked by arrow) rooted in the spot penumbra and an emerging parasitic field intrusion. LS2 is in the time interval $\langle RS, U \rangle$ (see Fig. 3) connected with lines of LS1. It hosts source SW of the 327 MHz pulses (see Fig. 6). In the background, there is the medium size arcade (shaded light grey) erupting during the impulsive phase.

same sources at low frequencies, but at 327 MHz a double source, one in LS1, and a correlated fluctuating source in LS2. The end of the second interval is characterized by the appearance of a decimetric type U burst at ≥ 400 MHz (second stippled line). This is also the end of the double source pattern of the BBP at 327 MHz. In the third interval the BBP source pattern is again simple, as in the first interval. But, there appears now a strong new feature – the zebra pattern (ZP) seen between about 220 and 140 MHz consisting of more than 20 stripes in emission and absorption, simultaneously. The source of the ZP is also situated in LS1.

Figure 4 is a more detailed plot of the feature called $dm\ BBP + F$ in Fig. 1 (arrow) as observed with the 48 channel spectral magnifier of AIP. The top left panel of Fig. 4 is the frequency average of all channels between 693 and 740 MHz. The decimeter patch consists of three intensity enhancements (like the main event, Fig. 1) with superposed fine structure. The further panels are pairwise combined of the dynamic spectra (left) and its time derivative (right). Three 2 s-intervals are given revealing fast BBP and $\approx 60\text{ MHz s}^{-1}$ drifting fiber bursts. The drift rate of the fibers becomes lower in the course of the patch.

In the next subsections we discuss the detailed spectral and spatial configuration of the BBPs as well as the ZPs.

2.2.1. Broad band pulsations

The BBP shown in Fig. 3 consists of more than 100 single pulses. If one checks the source configuration for the single

pulses – all pulses are observed at three different NRH frequencies – firstly the rough division into two basic source configurations comes into play. A typical “simply structured” pulse source is shown in Fig. 5.

The left panels in the figure show the space-time distribution of 327 MHz brightness as seen with the EW and the NS NRH scan. The inclination of the contour pattern reveals a mean source motion from SW toward NE. In the right panel start-, maximum- and end-positions of the 327 MHz source are shown by a black cross, a white dot (centroid) and a black/white stippled cross. The cross sequence in space suggests a motion. The distance between the initial and the final position is $\approx 0.12 R_{\odot}$ corresponding with an estimated projected speed of $\approx 1.1 \times 10^5\text{ km s}^{-1}$. The source is situated in the loop system LS1 in the NE of the active region as it turns out in the superposition with the SXT image. Because the LS1 field lines lead about in the same direction as the pulsed source, we conclude that the source motion within a single BB pulse is due to the motion of accelerated electrons along LS1 field lines. To get the observed repeated pulses a quasiperiodic particle injection into LS1 is necessary. As shown by Aurass et al. (1999) this is due to the flare-driven interaction between the LS1 field lines and the small field system between the parasitic polarity and the leading spot of AR 7792 (see also Fig. 2).

In Fig. 6 the situation at 327 MHz is shown for the time interval $\langle RS, U \rangle$ (Fig. 3). In this time, at the high frequency end of the pulses – with NRH only achieved at 327 MHz – there occurs a correlated double source. The subsources in LS1 shows in general the same properties as in the time before RS and after U. Also at low frequencies, the behaviour is coincident with those outside the interval. The newly formed SW source is $0.46 \dots 0.57 R_{\odot}$ away from the main (NE) source. This means the source distance is at least five times the source height above the photosphere. The SW source has about the same source extent as the NE source and fluctuates with more noise but is highly correlated with the main source. Possibly fluctuations in the contribution of the SW source are responsible for time variations of the high frequency envelope of the BBP. Despite the double source pattern the time profile of the single BB pulses remains sharply defined (see e.g. Fig. 6b). As expected for an exponential density–height profile, if the pulses result from plasma emission excited by a fast travelling exciter some pulses have a slightly turning branch at the low frequency end. We will quantitatively analyze the correlation of the flux of both subsources in Sect. 3. Aurass et al. (1999) concluded from the observations that in the interval $\langle RS, U \rangle$ of 90 s duration there remains only to assume a connection of the loop systems LS1 and LS2 with an electron acceleration site situated between both sources – in the active region – for understanding the complex situation. The connection to LS2 must be dissolved after 90 s. This follows because after the decimeter type U burst (Fig. 3) the BBP source configuration returns to the initial simple stage.

Of course in the late stage the formation of the zebra pattern source brings a new quality in the FS emission which we discuss in the next subsection. Before we should note that the two widely spaced sources at 327 MHz show a different sign of circular polarization. We found +30% (left handed) for the SW

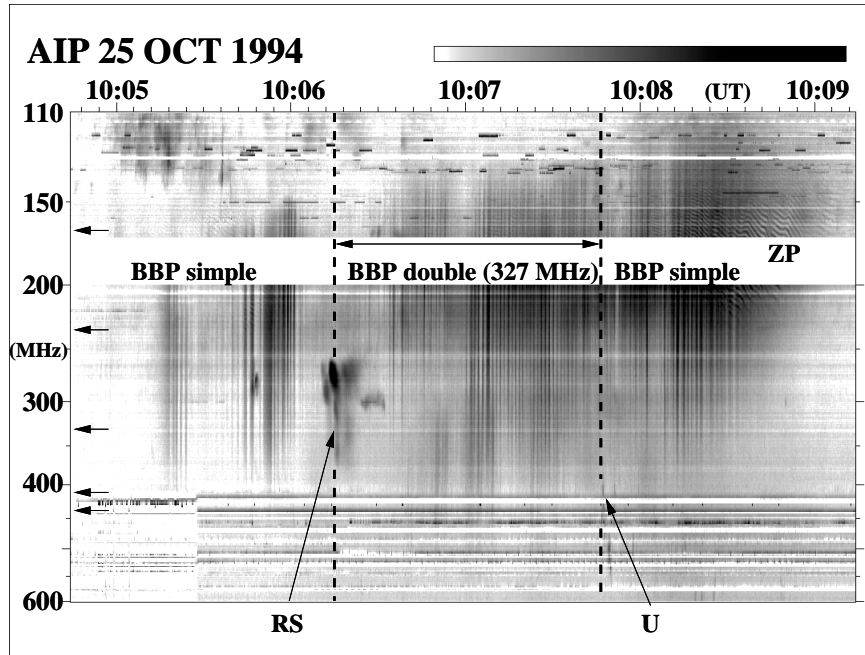


Fig. 3. Enlargement of fine structures between 10:05 and 10:09 UT. BBP – broad band pulsations; ZP – zebra pattern. Note the interval <RS, U> between the RS and the U burst (stippled lines and arrows).

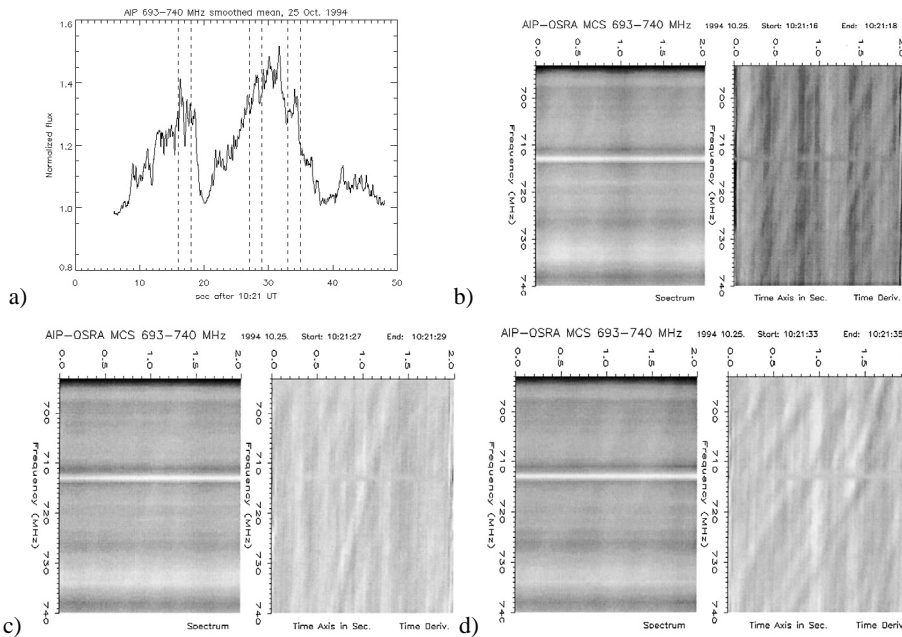


Fig. 4. The 693–740 MHz 48 channels (0.01 s sampling rate) spectrum of the 25 October 1994 late decimeter patch (see Fig. 1, arrow). **a)** The flux averaged over frequency (arb. units). **b)–d)** Sequence of three 2 s intervals marked by stippled lines on panel **a)**; left the spectrum, right its time derivative in each panel. Notice broad band pulsations and fiber (intermediate drift) bursts. During the event, the fiber burst drift rate decays.

source, and -40% (right handed) for the NE source. Accepting the leading spot hypothesis (e.g. Krüger 1979) the FS sources are polarized in the ordinary mode. This fact, together with the inclusion into the loop systems LS1 and LS2 led Aurass et al. (1999) to the conclusion that the BBP source is connected with the formation of a continuous sigmoid loop structure from the previously existing isolated northern and southern wing. We come back to this point in the discussion.

2.2.2. Zebra patterns

In contrast to the fast drifting type III bursts and BBP the ZP are characterized by a system of slowly drifting parallel lanes, bright, and almost equidistant in frequency. An enlargement out of the ZP patch at the low frequency side of the strong BBP (Fig. 1) is shown in Fig. 7 together with the NRH NS scans at 164 MHz. In the following we will find that despite the

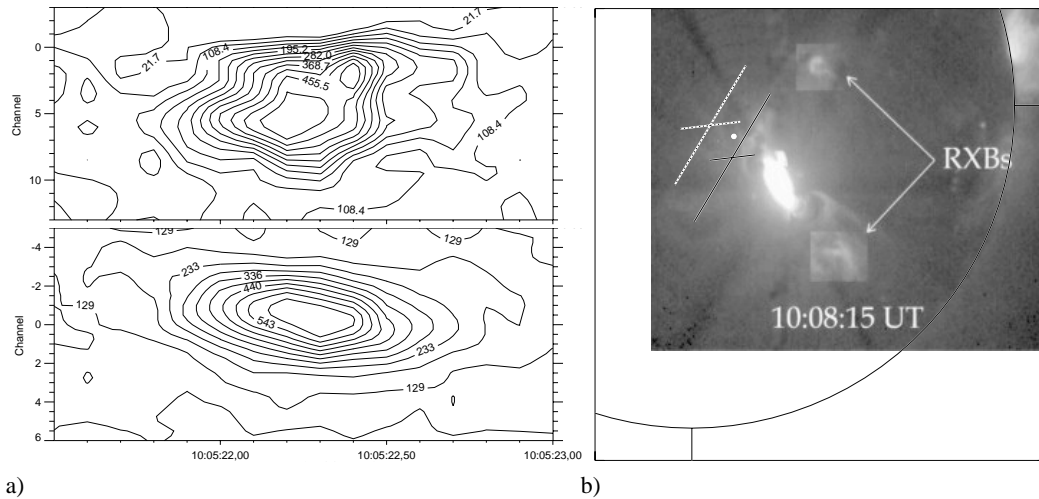


Fig. 5. Meter wave pulsation detail. The source (one pulse, here: 10:05:22 UT) at 327 MHz outside $\langle RS, U \rangle$ in Fig. 3. In **a)** contours of equal brightness over time; EW scan top, SN scan bottom. The vertical axes are graded in instrument-related units, corresponding to a field of $0.67 R_{\odot}$ in the upper panel, $1.08 R_{\odot}$ in the bottom panel. In **b)** position and source half width at pulse onset (21.84 s; solid cross) and end (22.64 s; dashed). Small white circle – centroid at maximum (22.24 s). The *Yohkoh* SXT image here and in following figures is from Manoharan et al. (1996). RXB means X-ray brightenings.

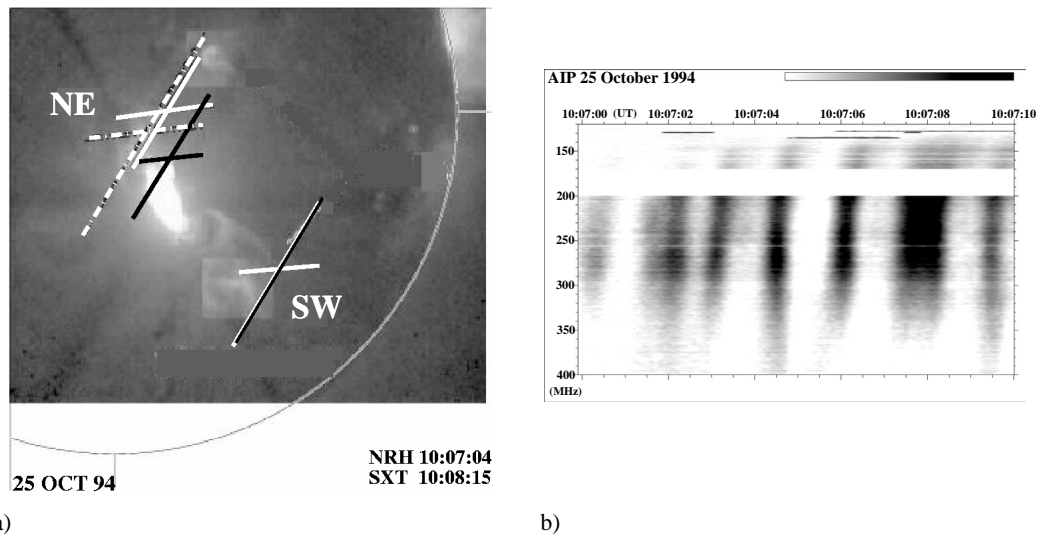


Fig. 6. Meter wave pulsation detail at 327 MHz in the interval defined by $\langle RS, U \rangle$ in Fig. 3. In **a)** the source configuration at 327 MHz. NE: main source site. Black cross: onset, white cross: end of the pulse. White-black stipple-dotted cross: source sites at 236.6 and 164 MHz. SW: pulsation source site with 90 s lifetime. In **b)** the spectrum of this and neighboring pulses. Notice the *J* burst behaviour at the low frequency edge, and see also Fig. 10.

extremely different spectrum (compared with BBP) the ZP source site is near those of BBPs in the active region.

Figure 7 reveals two facts. Firstly, in the early ZP (Fig. 7a) the BBP feature is still superposed leading to a quasi-periodic intensity rise in both stripes and gaps of the ZP. Secondly, there is a relation between the local stripe drift rate near the NRH observing frequency and the direction of the source motion. Negative drift rate (toward low frequencies, lower densities) means northward motion. Positive drift rate (toward high frequencies, higher densities) results in southward motion. The stronger the drift rate, the higher the speed of the motion. In

Sect. 3 we give a statistical analysis of the connection between stripe drift rate and source speed of the ZP.

In Fig. 8 we give two examples of the source sites during the excursion of a single zebra stripe across the 164 MHz NRH observing frequency level in the corona. Times are given so that the corresponding stripes can be compared in Fig. 7. As already noticed, different drift rate signs mean different source motion directions. The continuous cross is the ZP stripe onset, and the stippled cross is the stripe decay (bottom left only partially visible in the figure). In comparison with the source motion during a single BB pulse (Figs. 5 and 6) the source

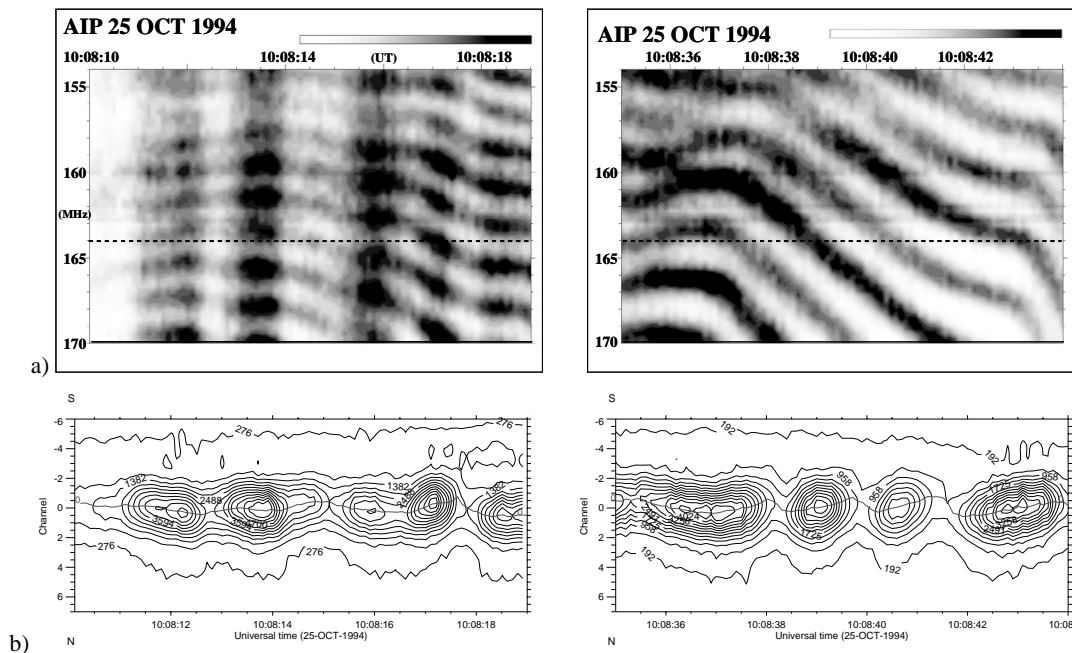


Fig. 7. Zebra pattern between 154 and 170 MHz. In **a)** spectra (AIP). The stippled line denotes 164 MHz. In **b)** the NRH 164 MHz contours of equal brightness, NS array. The vertical axis is graded in instrument-related units, corresponding to a field of $1.28 R_{\odot}$. The bold line gives the motion of the maximum of a Gaussian source model. Follow the stripes in the spectra and note the correlation of stripe inclination and source motion (see Fig. 11 for speed–drift rate statistics).

motion during a zebra stripe is more perpendicular to the dominant field line direction of LS1 (see Fig. 2), or, in other words the ZP source motion is orthogonal to the BBP source motion. In Fig. 8 we plot the source motion of a sample of stripes in heliographic coordinates. Some details become visible which do not alter our general statements. The zebra source is polarized in the same sense as the NE BBP source, and the degree of circular polarization is -26% (right handed).

3. Discussion

3.1. General aspects

The presented work is to our knowledge one of the first attempts to give detailed radio spectral and imaging information about the “elements” of the radio spectral FS BBP and ZP – the single pulsation pulse and the single zebra stripe. For both FS we found a moving radio source³ with a certain spatial orientation to the magnetic field direction in the surrounding corona as derived from a force-free extrapolation of the measured photospheric magnetic field.

The BBP source starts near the active region and decays away from it. The motion follows the predominant magnetic field direction, the apparent speed is a significant fraction of the speed of light. In a certain time interval and frequency range, the pulsating source appears branched at two widely separated subsources. From these observations we conclude that the radio emission is due to a moving exciter propagating along the field lines and being quasi-periodically injected in large scale magnetic field structures. Between the pulsating source and the

injection site, the exciter passes sometimes a magnetic branch point between the loop systems LS1 and LS2 (Fig. 2).

In contrast, the zebra stripe source starts moving at one of the two “transverse” edges of the magnetic field structure hosting both FS sources (here: LS1). The motion is transverse to the dominant magnetic field direction. If the zebra stripe crosses the observing frequency level in the dynamic spectrum with nonzero inclination the source motion is well defined. Again, the apparent speed is a significant fraction of the speed of light. Changing the sense of the spectral drift rate corresponds with changing the sense of source motion.

We claim that both results together can be understood only by the mechanism of repeated injection of nonthermal electrons into an asymmetric magnetic trap. The injection should happen near the high-field footpoint of the trap. Specifically the branch point observation, the high speeds and the single pulsation pulse spectral properties reveal nonthermal electrons as the exciting agent, and a type III like emission mechanism in a closed field configuration for the single pulse radio radiation. Due to our pre-knowledge about the flare of 25 October 1994 (Aurass et al. 1999) we argue that the mechanism of repeated injection of bunches of electrons is the flare-driven interaction of LS1 with the extremely small-scale loop system formed above a parasitic intrusion of emerging flux near to the leading spot of AR 7792 (Fig. 2, arrow). In Paper II we will compare the different BBP models with the observations. Further, we will demonstrate in Paper II that the ZP mechanism of double plasma resonance (Zhelesnjakov & Zlotnik 1975) generally and in many details explains the presented data, and that both the preferred BBP and the ZP mechanisms are natural properties of the given asymmetric trap. First, some attempts to

³ Such a finding was already mentioned for ZP sources by Chernov et al. (1994).

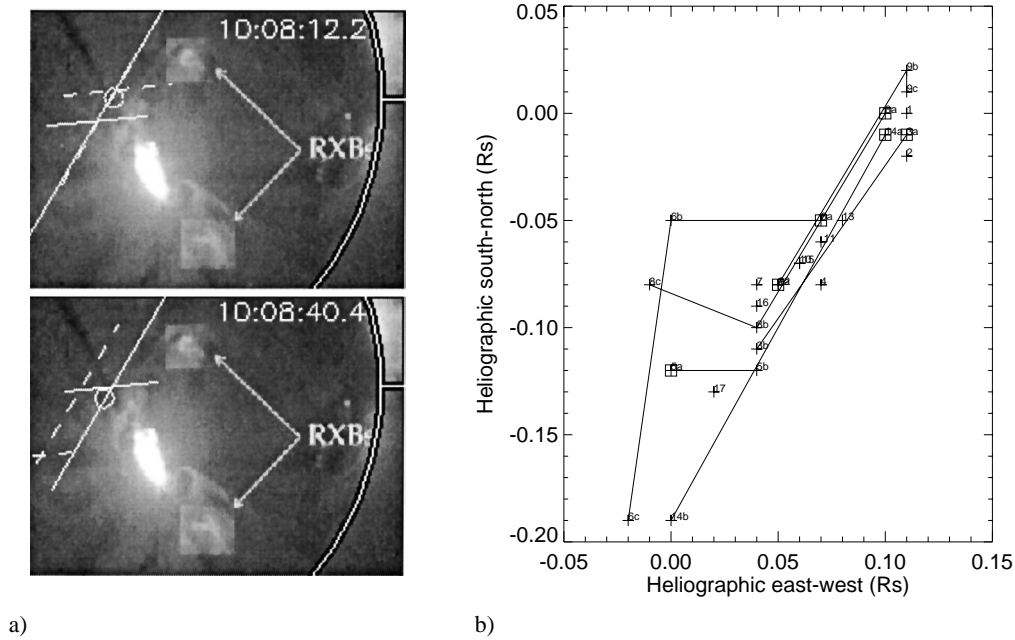


Fig. 8. Zebra pattern detail. **a)** Source sites of two stripes showing both observed drift directions; cross: onset, stippled cross: decay of the source. Circle: source centroid at peak intensity, circle size: beam width. Compare with the stripe drift rates in Fig. 7. **b)** Motion of the centroid of stripe sources at the peak of emission (plus signs). Positions are labelled in sequence of cutting the 164 MHz level (No. 1 – 10:08:12.2). Sources of the same stripe are connected, letters a, b, c – labels in time sequence. Plus signs in squares – first of successive sources of the same stripe.

quantify the conclusions from the data by means of statistical methods will be presented here.

3.2. Statistical analysis

Firstly we will characterize the different BBP signatures by a power spectral representation. Then, we will compare the statistics of both the components of the 327 MHz pulsation by a cross correlation analysis. Finally we will check if there is a systematic dependence between the zebra stripe frequency drift rate and the projected speed measured in the corresponding stripe radio source.

3.2.1. Pulsation power spectral analysis

We have two samples of quasiperiodic broad band radio flux oscillations. In the meter wave range we use for the power spectral analysis only the flux of the NE source (Fig. 6) at all three relevant NRH frequencies. In the decimeter wave range we first suppressed slowly drifting features (fiber bursts) by averaging all 48 channels over frequency.

Both data sets were transformed to the smoothed time derivative of the flux records to reject linear trends. A next step was the autocorrelation analysis, the correlation function was Hanning-windowed with a correlation length of 50 and 150 samples, respectively (for methodical details e.g. Jenkins & Watts 1968). Figure 9 gives the results. There is no significant difference in the spectral data for the three NRH frequencies. This was expected for a broad band fast drift phenomenon. The period of the meter wave pulsations amounts

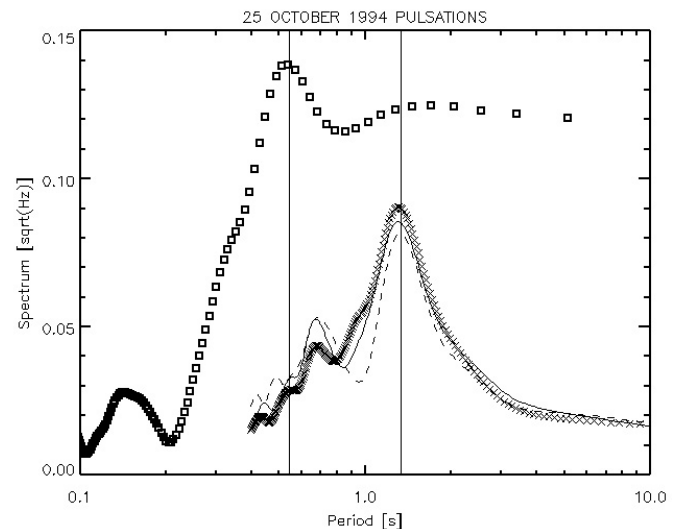


Fig. 9. Power spectrum of broad band pulsations. Squares: frequency range 693–740 MHz 10:21:06–10:21:48 UT, see also Fig. 1, and Fig. 4. The period is 0.54 s. Crosses, line and stippled line: NRH 164, 236.6 and 327 MHz; only the NE source flux (see Fig. 6). The period is 1.33 s.

to 1.33 ± 0.03 s. The period of the decimetric pulsations is 2.5 times smaller – from the spectrum one reads 0.54 ± 0.05 s. Both pulse periods are clear in the spectra, therefore we did not draw significance levels in the figure.

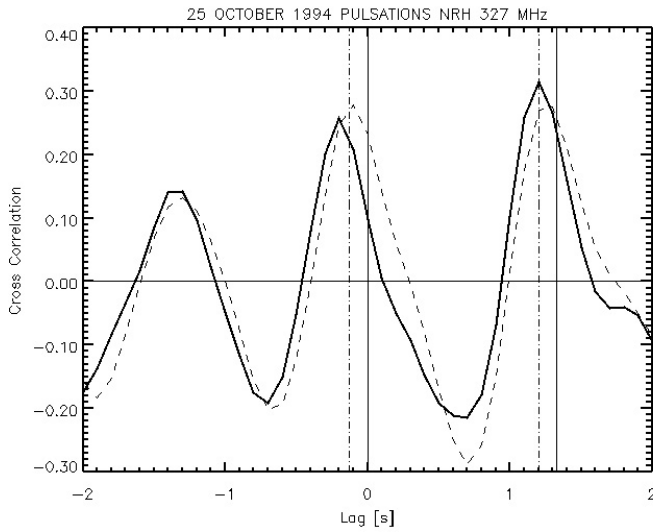


Fig. 10. Cross correlation function (after detrending and 0.3 s smoothing) between NE (cont.) and SW (stippl.) source of Fig. 6 taken in $\langle RS, U \rangle$ of Fig. 3. Continuous vertical lines mark one m-BBP period of 1.33 s. stippled lines are the same shifted by -0.13 s.

3.2.2. Pulsation cross correlation analysis

Thanks to the high time resolution of the NRH, and due to the wide spacing between the both simultaneously fluctuating sources at 327 MHz (NE and SW in Fig. 6) both sources are independently observed. By a cross correlation analysis of the separate fluctuation records from both source sites we will learn more about the source split observed in the interval $\langle RS, U \rangle$ Fig. 3. We treated the data of the EW and the NS scans separately. The result is shown in Fig. 10.

In both scans, the best correlation between the time series is at $-(0.1 \dots 0.2)$ s, and at $+(1.2 \dots 1.3)$ s. As expected, the distance between the lag values of maximum correlation is just one full period (which was 1.33 s). This supports our assumption that the fluctuations at both sources are driven by the same source of nonthermal electrons. It also supports our conclusion that for the time of the source split detected at NRH 327 MHz there must be a magnetic branch point on the electron paths between the injection site and the radio sources in loop systems LS1 and LS2. This fact is strong evidence for the formation of a magnetic connection and (90 s later) disconnection between field lines of both loop systems and the acceleration site. As we know (Fig. 3) this connection and disconnection is associated with specific decimetric burst features in the radio spectrum. We have discussed this point in detail in Aurass (1999) and gave a model of the resulting field line connectivity during the flare. From the lag time, and the delays with respect to zero lag, we can reconfirm the injection site because we know the (mean) projected difference between the source centroids of the NE and the SW source ($0.46 \dots 0.57 R_{\odot}$), let's assume 360.5 Mm. We know that the injection site of the nonthermal electrons is nearer to the NE source. The distance between NE and SW is, according to the correlation maxima on the lag scale, divided in the ratio (0.15/1.25). Therefore the injection site is on average over all pulses in the interval $\langle RS, U \rangle$ situated 43.3 Mm (59.5 arcsec) southwest of the mean

Table 1. The data shown in Fig. 11. Event 25 October 1994 – NRH heliographic positions of ZP sources, speeds of the source motion at 164 MHz, and instantaneous drift rates of the ZP stripes in the AIP dynamic spectrum. No. – arbitrary running stripe number. Pos. – NRH positions, 0 refers to disk centre. Drift rates in brackets are not strictly local at 164 MHz.

No.	Peak (UT) (in 10:08)	Pos. (R_{\odot})		Speed (10^5 km s^{-1})	D_f (MHz s^{-1})
		EW	NS		
1	12:212	0.11	0.00	0.84	-0.71
2	13:812	0.11	-0.02	0.23	0.64
3a	15:912	0.11	-0.01	0.53	pulsation
3b	17:112	0.04	-0.11	-1.87	2.30
4	19:612	0.07	-0.08	-1.20	1.41
5a	21:212	0.00	-0.12	-1.86	1.70
5b	22:512	0.04	-0.12	-2.28	2.06
6a	23:912	0.07	-0.05	-1.00	5.89
6b	25:712	0.0	-0.05	-0.86	0
6c	26:812	-0.02	-0.19	0.06	0
7	28:512	0.04	-0.08	-0.65	1.55
8a	29:912	0.10	0.00	2.55	1.50
8b	30:512	0.04	-0.10	-0.96	1.54
8c	32:112	-0.01	-0.08	0.11	0
9a	34:412	0.05	-0.08	-1.03	0 (2.03)
9b	36:912	0.11	0.02	1.09	<0 (-0.58)
9c	37:012	0.11	0.01	-1.49	>0 (2.54)
10	38:912	0.06	-0.07	-1.10	2.43
11	40:512	0.07	-0.06	-1.66	2.30
12	43:012	0.05	-0.08	-1.01	0
13	44:912	0.08	-0.05	-0.45	6.67
14a	47:812	0.10	-0.01	-1.93	1.43
14b	50:312	0.00	-0.19	-0.24	0
15	51:912	0.06	-0.07	-2.76	2.80
16	53:512	0.04	-0.09	-2.86	2.58
17	55:112	0.02	-0.13	-1.97	2.66

NE source site. This is a guess, only, but in agreement with our interpretation of the magnetic field and loop structure above AR 7792.

3.2.3. Zebra stripe regression analysis

The systematic connection between the sign of the local zebra stripe drift rate near the NRH imaging frequency and the sign of the speed of the apparent stripe source motion on the solar disc (Fig. 8) is evident. The regression plot is shown in Fig. 11. The figure presents the drift rate – speed sample with minor modifications. A linear regression represents the data points. This reveals a statistically founded simple relation between the spectral drift rate and the source speed. The signs were chosen according to the usual solar radio standards. Like the northeastern BBP source, the zebra source is situated near the NE turning branch of the soft X-ray sigmoid. The stripe 10:08:12 moves from SE to NW. A negative stripe drift rate is observed revealing a motion from higher to lower densities. In contrast, the stripe 10:08:40 moves from NW to SE, showing a positive stripe drift rate and a source motion from low to high densities.

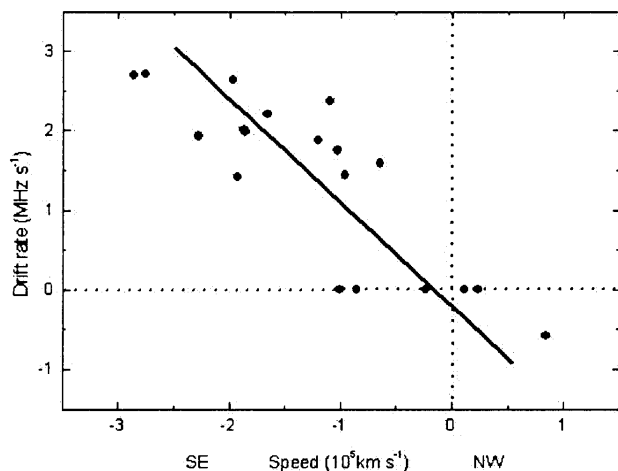


Fig. 11. Relation between the projected zebra stripe source speed (comp. Fig. 8) and the stripe drift rate in the spectrum at 164 MHz. See Appendix for the data. The sample was cleaned from four points with undefined drift rate and two points with extreme drift rate excursion.

4. Conclusions

The aim of Paper I was the analysis of the radio fine structure data observed during the type IV burst of 25 October 1994 focusing on the spectral and spatial properties of broad band pulsations and zebra patterns during this well-analyzed event. We presented spectral and imaging data of single pulses and zebra stripes, as well as results of a statistical analysis of the FS patches in the given event. We found evidence to conclude that probably both the BBP and the ZP are due to repeated nonthermal electron injection into an asymmetric magnetic trap. A common driving agent for both FS would be in good accord with the mostly coupled occurrence of both FS varieties. From our previous knowledge of the magnetic field configuration of the flaring active region (Aurass et al. 1999) we believe that the reason for the repeated electron injection is a flare-induced interaction between a small-scale and a large-scale magnetic field line system. At least in the analyzed event it is evident that the BBP pulses are beam-driven emission out of a closed but asymmetric magnetic field configuration. This is in accordance with the predictions of Kuijpers (1980) about quasi-period particle injection as a possible driver of FS emission, but in contrast with the results of Aschwanden & Benz (1986) who exclude after studying data at 650 MHz a type III-like mechanism for BBP. In a next paper (Paper II) we will compare the predictions of different BBP models with our observations to consolidate our conclusion. Further, we will reconsider some details of the data to confirm that the zebra pattern is due to the plasma double resonance mechanism in the same flux tube which also hosts the pulsation source. Therefore, Papers I and II together give answers to a series of long-standing questions about the nature of solar type IV radio burst fine structures.

Acknowledgements. H.A. is grateful to B. Vršnak, S. Kahler and M. Karlicky for comments about the manuscript. E.Y.Z. and V.V.Z. are supported by the RFBR (02-02-04005) and the DFG (436RUS 113/675/2-1 R). We acknowledge L. van Driel-Gesztelyi and the *Astrophysical Journal* for the kind permission to use the Yohkoh-SXT image in Figs. 5, 6, and 8. The Nançay Radio Observatory is funded by

the French Ministry of Education, the CNRS and the Région Centre. The authors thank the referee, Dr. Jan Kuijpers, for his interest and constructive remarks.

References

- Abrami, A., & Koren, U. 1978, *A&AS*, 34, 165
 Aschwanden, M. J. 1987, *Sol. Phys.*, 111, 113
 Aschwanden, M. J., & Benz, A. O. 1986, 158, 102
 Aurass, H. 1999, in ed. T. Bastian, N. Gopalswamy, & K. Shibasaki, *Solar Physics with Radio Observations*, NRO Report, 479, 293
 Aurass, H., & Chernov, G. 1983, *Sol. Phys.*, 84, 339
 Aurass, H., Chernov, G., Karlický, M., Kurths, J., & Mann, G. 1987, *Sol. Phys.*, 112, 347
 Aurass, H., & Klein, K.-L. 1997, *A&AS*, 123, 279
 Aurass, H., Mann, G., Hanschur, U., & Zlobec, P. 2000, *Hvar Obs. Bull.* 24, 165
 Aurass, H., Vourlidas, A., Andrews, M. D., et al. 1999, *ApJ*, 511, 451
 Aurass, H., Vršnak, B., Hofmann, A., & Rudžjak, V. 1999, *Sol. Phys.*, 190, 267
 Bastian, T., Pick, M., Kerdraon, A., Maia, D., & Vourlidas, A. 2001, *ApJ*, 558, L65
 Chernov, G. P., Markeev, A. K., & Korolev, O. S. 1975, *Sol. Phys.*, 44, 435
 Chernov, G. P. 1976, *Sov. Astron. J.*, 20, 449
 Chernov, G. P., Klein, K.-L., Zlobec, P., & Aurass, H. 1994, *Sol. Phys.* 155, 373
 Chernov, G. P., Markeev, A. K., Poquérousse, et al. 1998, *A&A*, 334, 314
 Gotwols, B. L. 1973, *Sol. Phys.*, 33, 475
 Elgarøy, Ø. 1959, *Nature*, 184, 885
 Ellis, G. R. A. 1969, *Aust. J. Phys.*, 22, 177
 Jenkins, G. M., & Watts, D. G. 1968, *Spectral Analysis and Its Applications* (San Francisco: Holden Day-Series in Time Series Analysis)
 Kai, K., & Takayanagi, A. 1973, *Sol. Phys.*, 29, 461
 Karlický, M., Fárník, F., & Meszárosóvá, H. 2002, *A&A*, 395, 677
 Khan, J., Vilmer, N., St. Hilaire, P., & Benz, A. 2002, *A&A*, 388, 363
 Klein, K. L., Aurass, H., Soru-Escout, I., & Kálmán, B. 1997, *A&A*, 320, 612
 Krüger, A. 1979, *Introduction to Solar Radio Astronomy and Radio Physics* (Dordrecht: Reidel)
 Kuijpers, J. 1975a, *A&A*, 40, 405
 Kuijpers, J. 1975b, *Sol. Phys.*, 44, 173
 Kuijpers, J. 1980, in *Radio Physics of the Sun*, IAU Symp. 86, ed. M. Kundu, & T. Gergely (Dordrecht, Reidel), 341
 Mann, G., Aurass, H., Voigt, W., & Paschke, J. 1992, *ESA Journal*, SP-348, 129
 Manoharan, P. K., van Driel-Gesztelyi, L., Pick, M., & Démoulin, P. 1996, *ApJ*, 468, L73
 McLean, D. J., & Sheridan, K. V. 1973, *Sol. Phys.*, 23, 485
 McLean, D. J., & Labrum, N. R. 1985, *Sol. Radiophys.* (Cambridge: Cambridge Univ. Press)
 Rosenberg, H. 1970, *A&A*, 9, 159
 Slottje, C. 1972, *Sol. Phys.*, 25, 210
 Slottje, C. 1981, *Atlas of Fine Structures of Dynamic Spectra of Solar Type IV-dm and Some Type II Radio Bursts* (Utrecht: Publ. Utrecht Observatory)
 The Radioheliograph Group 1993, *Adv. Sp. Res.*, 13(9), 411
 Trottet, G., Kerdraon, A., Benz, A. O., & Treumann, R. 1981, *A&A*, 93, 129
 Winglee, R. M., & Dulk, G. A. 1986, *ApJ*, 307, 808
 Young, C. W., Spencer, C. L., Moreton, G. E., & Roberts, J. A. 1961, *ApJ*, 133, 243
 Zheleznyakov, V. V., & Zlotnik, E. Ya. 1975a, *Sol. Phys.*, 43, 431; 1975b, 44, 461